Article

Amine-Functionalized Task-Specific Ionic Liquids: A Mechanistic Explanation for the Dramatic Increase in Viscosity upon Complexation with CO from Molecular Simulation

Keith E. Gutowski, and Edward J. Maginn

J. Am. Chem. Soc., **2008**, 130 (44), 14690-14704 • DOI: 10.1021/ja804654b • Publication Date (Web): 11 October 2008

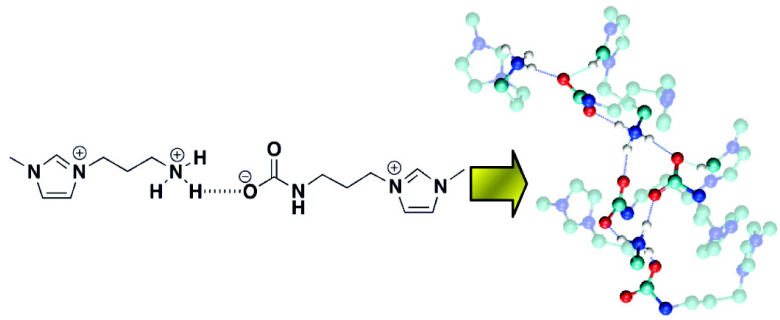

More About This Article

Additional resources and features associated with this article are available within the HTML version:

- Supporting Information
- Access to high resolution figures
- Links to articles and content related to this article
- Copyright permission to reproduce figures and/or text from this article

View the Full Text HTML

J|A|C|S
ARTICLES

Published on Web 10/11/2008

Amine-Functionalized Task-Specific Ionic Liquids: A Mechanistic Explanation for the Dramatic Increase in Viscosity upon Complexation with CO_2 from Molecular Simulation

Keith E. Gutowski and Edward J. Maginn*

Department of Chemical and Biomolecular Engineering, University of Notre Dame, 182 Fitzpatrick Hall, Notre Dame, Indiana 46556

Received June 24, 2008; E-mail: ed@nd.edu

Abstract: The capture of CO_2 from fossil fuel combustion, particularly in coal-fired power plants, represents a critical component of efforts aimed at stabilizing greenhouse gas levels in the atmosphere. Alkanolamines have traditionally been used to this end; however, drawbacks such as volatility, degradation, and regeneration costs have been drivers for the development of new, superior technologies. Recently, several seminal studies with ionic liquids (ILs), both experimental and computational, have demonstrated their potential as CO_2 capture agents. In traditional ILs, experimental studies with CO_2 have revealed its unusually high physical solubility in these media. Complementary simulation studies have provided evidence that this is attributable to CO_2 occupying void space within the liquid and favorably interacting with the anion. Recently, a series of second-generation task-specific ionic liquids (TSILs) containing amine functional groups have been synthesized and demonstrated to have much higher capacities for CO_2 due to their reactivity with CO_2, as well unusually high viscosities in both the neat and complexed states. The current work extends the seminal studies of CO_2 capture with ILs by providing insight from simulations into the mechanism responsible for the dramatic increase in viscosity upon complexation. Simulations conclusively demonstrate that the slow translational and rotational dynamics, which are manifest in the high viscosity, may be attributable to the formation of a strong, pervasive hydrogen-bonded network. Semiquantitative estimates of the cation and anion self-diffusion coefficients and rotational time constants, as well as detailed hydrogen bond analysis, are consistent with the experimentally observed formation of glassy or gel-like materials upon contact with CO_2. This has significant implications for the design of new approaches or materials involving ILs that take advantage of these preconceived limitations, in the synthesis or manipulation of new TSIL frameworks for CO_2 capture, and in novel experimental studies of chemistries and dynamics in persistent heterogeneous environments.

Introduction

Recent concerns over global warming due to greenhouse gas emissions from fossil fuel combustion have resulted in global efforts to develop more effective and efficient ways to sequester these gases prior to atmospheric release. It has been noted that, in the early 2000s, a sharp acceleration in global emissions occurred, and that the dominant factor behind the recent rapid growth in atmospheric CO_2 (>2 ppm/year) is high and rising emissions.[1] In 2005, the Energy Information Administration reported that global emissions of CO_2 from the consumption and flaring of fossil fuels was 28.2 billion metric tons.[2] Considering these staggering statistics, it is no surprise that the efficient removal and subsequent sequestration of CO_2 from postcombustion emission streams is viewed by many as a critical component of efforts aimed at stabilizing atmospheric CO_2 levels. The flue gas produced from the combustion of coal is typically composed of a mixture of gases, including CO_2, NO_x, SO_x, H_2S, and N_2, with CO_2 comprising about 12% of the mixture.[3] One approach being considered for capturing CO_2 is the use of liquid absorbents designed to selectively solvate CO_2. However, many criteria must be considered when choosing or developing absorbents for CO_2 removal, including selectivity, cost, and stability. Scale of operations would require that absorbents have the capacity and durability to handle approximately 2.5 million tons of CO_2 per year, the average output from an existing 450 MW coal-fired power plant.[4] Current state-of-the art technology uses dilute aqueous solutions of alkanolamines, primarily monoethanolamine (MEA), in the sequestration process.[5] MEA is advantageous due to its high reactivity, low cost, high absorption capacity on a weight basis, and reasonable thermal stability. However, the use of MEA at large

(1) Raupach, M. R.; Marland, G.; Ciais, P.; Le Quéré, C.; Canadell, J. G.; Klepper, G.; Field, C. B. *Proc. Natl. Acad. Sci. U.S.A.* **2007**, *104*, 10288–10293.
(2) DOE/EIA. International Energy Annual 2005; Energy Information Administration: Washington, DC, 2005.
(3) McCann, N.; Maeder, M.; Attalla, M. *Ind. Eng. Chem. Res.* **2008**, *47*, 2002–2009.
(4) DOE/NETL. Carbon Dioxide Capture from Existing Coal-Fired Power Plants. Technical Report No. DOE/NETL-401/110907; National Energy Technology Laboratory: November 2007.
(5) Alejandre, J.; Rivera, J. L.; Mora, M. A.; de la Garza, V. *J. Phys. Chem. B* **2000**, *104*, 1332–1337.

10.1021/ja804654b CCC: $40.75

fossil fuel power plants is largely hindered by its high enthalpy of reaction and hence high energy demand for regeneration, as well as susceptibility to oxidative degradation and corrosion concerns.[3,6]

Recently, attention has focused on the use of chilled ammonia as an alternative to alkanolamines for the capture of CO_2. Reaction of CO_2 with NH_3 results in the formation of ammonium bicarbonate. Low temperatures (0−10 °C) are needed to prevent the vaporization of NH_3 and loss of absorbent and to optimize conditions for the formation of solid ammonium bicarbonate. Ammonia has several advantages over aqueous amines including lower cost, higher CO_2 capacity, lower decomposition temperature of the ammonium bicarbonate product, and a less corrosive environment.[7] In addition, a tremendous amount of information exists regarding solution equilibria of carbonate systems.[8] However, cooling the systems adds to energy usage and operation costs, and the generation of solid ammonium bicarbonate complicates engineering design.[7]

The mechanism of the reaction between CO_2 and aqueous solutions of amines has been studied experimentally. Caplow[9] and Danckwerts[10] have both proposed a two-step mechanism, also known as the zwitterion mechanism, where a stable zwitterion intermediate is proposed to exist in solution, as in eqs 1 and 2. In eq 2, the proton from the zwitterion is transferred

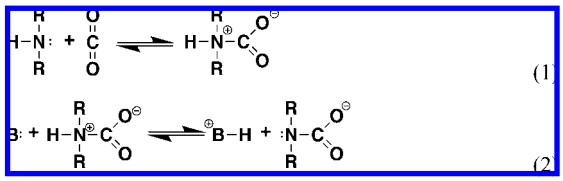

(1)

(2)

to a base (B), which may be a water molecule, an additional amine, or any other basic species. Using rate constant data, Crooks and Donnellan[11] suggested that the Danckwerts mechanism was unlikely, and rather a concerted, single-step termolecular mechanism was more plausible, as in eq 3. Regardless

(3)

of mechanism, a carbamate and a protonated base are the generally accepted products of this reaction. In addition to reaction of CO_2 with an amine, a reaction can also occur between CO_2 and water in the aqueous system to form carbonic acid and bicarbonate. Computational chemistry has been used to provide mechanistic insight into the CO_2−amine reaction. da Silva and Svendsen have used ab initio calculations coupled with continuum solvation models to provide evidence that supports the single-step, termolecular reaction mechanism (eq 3) and that a zwitterion intermediate is likely to be short-lived.[12,13] In addition, they have shown that carbamate stability can be reasonably modeled using density functional theory (DFT) coupled with free energy perturbation methods.[6] Arstad et al. used molecular orbital (MO) theory and DFT to provide mechanistic insight into the CO_2−amine reaction, emphasizing the catalytic effect that water, ammonia, or alkanolamines may have on the reaction kinetics.[14]

Although aqueous alkanolamines and ammonia have found, and will continue to find, use in CO_2 scrubbing applications, there is a driving force to develop new alternatives to these materials that circumvent some of the drawbacks that plague their use and implementation. Recently, a large number of experimental solubility studies on gases such as CO_2, N_2, O_2, and SO_2 have been performed in ionic liquids (ILs).[15−17] ILs can be designed to possess low to negligible vapor pressure, enhanced thermal stability, and wide liquidus windows, thus minimizing the effects of absorbent loss and degradation.[18] Interestingly, it has been demonstrated that the physical solubilities of SO_2 and CO_2 in imidazolium-based ILs are remarkably high, while N_2 and O_2 are only sparingly soluble. For instance, in 1-butyl-3-methylimidazolium hexafluorophosphate, CO_2 is soluble up to 50 mol % at 50 bar of CO_2 pressure, and this behavior has been confirmed in a large number of different ILs.[16,17] Molecular simulations have also been performed that have aided in understanding the important interactions that contribute to the high solubility of CO_2. Results from our group[17,19] and those of others[20] provide evidence for negligible volume expansion and little liquid structure alteration upon absorbing CO_2, thus suggesting that the free volume or empty cavity space accommodates the CO_2 molecules. It is also observed that the CO_2 molecules have a greater affinity for anion versus cation associations, further supporting experimental evidence for a greater anion effect in CO_2 solubility.[16]

Recently, Bates et al.[21] proposed the use of task-specific ionic liquids (TSILs), specifically ILs that have been chemically modified to contain an amine functional group, as CO_2 absorbents. Bates et al. synthesized the TSIL, 1-(3-aminopropyl)-3-*n*-butylimidazolium tetrafluoroborate, and proposed a one-step CO_2 reaction mechanism in accordance with that of Crooks and Donnellan.[11] On the basis of FT-IR and ^{13}C NMR evidence, it was suggested that the base (B) is an additional TSIL cation, thus forming carbamate (zwitterion) and quaternary ammonium (dication) species, resulting in a 2:1 TSIL:CO_2 reaction stoichiometry.

It has been observed experimentally by Soutullo and coworkers that amine-functionalized TSILs have relatively high viscosities in the pure state, but upon contact with CO_2 the viscosity increases dramatically, forming a gel-like substance.[22] Yu and co-workers[23] used molecular simulations to help explain

(6) da Silva, E. F.; Svendsen, H. F. *Ind. Eng. Chem. Res.* **2006**, *45*, 2497–2504.
(7) You, J. K.; Park, H.; Yang, S. H.; Hong, W. H.; Shin, W.; Kang, J. K.; Yi, K. B.; Kim, J.-N. *J. Phys. Chem. B* **2008**, *112*, 4323–4328.
(8) Wen, N.; Brooker, M. H. *J. Phys. Chem.* **1995**, *99*, 359–368.
(9) Caplow, M. *J. Am. Chem. Soc.* **1968**, *90*, 6795–6803.
(10) Danckwerts, P. V. *Chem. Eng. Sci.* **1979**, *34*, 443–446.
(11) Crooks, J. E.; Donnellan, J. P. *J. Chem. Soc., Perkin Trans. 2* **1989**, 331–333.
(12) da Silva, E.; Svendsen, H. F. *Ind. Eng. Chem. Res.* **2004**, *43*, 3413–3418.
(13) da Silva, E.; Svendsen, H. F *Int. J. Greenhouse Gas Control I* **2007**, *15*, 1–157.
(14) Arstad, B.; Blom, R.; Swang, O. *J. Phys. Chem. A* **2007**, *111*, 1222–1228.
(15) Anthony, J. L.; Maginn, E. J.; Brennecke, J. F. *J. Phys. Chem. B* **2002**, *106*, 7315–7320.
(16) Anthony, J. L.; Anderson, J. L.; Maginn, E. J.; Brennecke, J. F. *J. Phys. Chem. B* **2005**, *109*, 6366–6374.
(17) Cadena, C.; Anthony, J. L.; Shah, J. K.; Morrow, T. I.; Brennecke, J. F.; Maginn, E. J. *J. Am. Chem. Soc.* **2004**, *126*, 5300–5308.
(18) *Ionic Liquids in Synthesis*, 2nd ed.; Wasserscheid, P., Welton, T., Eds.; Wiley VCH: Weinheim, 2007.
(19) Shi, W.; Maginn, E. J. *J. Phys. Chem. B* **2008**, *112*, 2045–2055.
(20) Huang, X.; Margulis, C. J.; Li, Y.; Berne, B. J. *J. Am. Chem. Soc.* **2005**, *127*, 17842–17851.
(21) Bates, E. D.; Mayton, R. D.; Ntai, I.; Davis, J. H., Jr. *J. Am. Chem. Soc.* **2002**, *124*, 926–927.
(22) Soutullo, M. D.; Odom, C. I.; Wicker, B. F.; Henderson, C. N.; Stenson, A. C.; Davis, J. H, Jr. *Chem. Mater.* **2007**, *19*, 3581–3583.

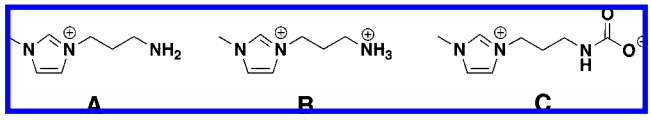

Figure 1. Cation (**A**), dication (**B**), and zwitterion (**C**) species.

the high viscosity of the neat TSILs. They found that the anions prefer to interact strongly with the $-NH_2$ tails of the cations via hydrogen bonding, which they suggest leads to the high viscosity. The dramatic increase in viscosity upon contacting these materials with CO_2 greatly impacts the way these materials might be used for CO_2 capture. The mechanism for the viscosity increase in the amine-functionalized TSILs has not been thoroughly investigated, although strong evidence exists for the formation of salt bridges,[22] consistent with the work of Rukevich and co-workers on amine-tethered supramolecular complexes. Rudkevich and co-workers have demonstrated that supramolecular frameworks, primarily based on calixarenes that have been tethered with amine groups, reversibly bind with CO_2 forming cross-linked polymers that can have gel-like properties. Substantial NMR and spectroscopic evidence supports the formation of carbamate and ammonium tails that participate in salt-bridges that form both linear supramolecular aggregates and three-dimensional supramolecular networks.[24]

Studying the absorption and subsequent reaction of CO_2 with amine-functionalized TSILs provides a particular challenge for molecular simulations. In this study, we use molecular dynamics to study the physical properties and dynamics of the pure and CO_2-reacted TSIL systems. Force fields are proposed for a new amine-functionalized TSIL, 1-(3-aminopropyl)-3-methylimidazolium bis(trifluoromethanesulfonyl)imide (Tf_2N^-), as well as for the dication and zwitterion derivatives of the TSIL cation representing the proposed reacted species according to the Crooks and Donnellan mechanism. The cation (**A**), dication (**B**), and zwitterion (**C**) are illustrated in Figure 1. The standard Tf_2N^- anion is not shown and has the chemical formula $(CF_3SO_2)_2N^-$. Different mixture compositions (**A**:**B**:**C**) are simulated, representing mixtures at various states of conversion from unreacted (all **A**) to fully reacted (no **A** and equal parts **B** and **C**). The effect of water was also studied by carrying out simulations with (wet) and without (dry) water present. Liquid structure as well as translational and rotational dynamics are computed at each composition and used to explain the observed experimental viscosity trends.

Force Field Development

Classical force fields were developed for the total energy, V_{tot}, assuming the functional form shown in eq 4. Separate terms are given for the energy contribution due to bonds, angles, dihedrals, impropers, van der Waals interactions, and Coulombic interactions, respectively.

$$V_{tot} = \sum_{bonds} k_b(r - r_0)^2 + \sum_{angles} k_\theta(\theta - \theta_0)^2 + \sum_{dihedrals} k_\chi[1 + \cos(n\chi - \delta)] + \sum_{impropers} k_\psi(\psi - \psi_0)^2 + \sum_{i=1}^{N-1}\sum_{j>i}^{N}\left\{4\varepsilon_{ij}\left[\left(\frac{\sigma_{ij}}{r_{ij}}\right)^{12} - \left(\frac{\sigma_{ij}}{r_{ij}}\right)^{6}\right] + \frac{q_i q_j}{4\pi\varepsilon_0 r_{ij}}\right\} \quad (4)$$

The parameters and corresponding atom types are provided in the Supporting Information. Force field (FF) parameters for eq 4 were obtained in the following manner. Parameters for the Tf_2N^- anion were taken directly from the work of Canongia Lopes and Padua and used without modification.[25] Equilibrium bond distances (r_0) and angles (θ_0) for the heterocycles **A**, **B**, and **C** were obtained from geometry optimizations at the B3LYP/6-311+G* level of theory[26] using the Gaussian03 suite of programs.[27] The optimized gas-phase structure of **C** with no constraints results in a structure in which the alkyl chain wraps around to facilitate a short carbamate oxygen atom hydrogen-bonding interaction with the acidic C2 hydrogen atom of the imidazolium ring, the lowest energy interaction in the gas phase. However, this interaction is not likely to occur in the liquid phase, and neighboring interactions would dominate. Thus, a constrained optimization of **C** was performed where the dihedrals CPH2−NR1−CN7B−CT2, NR1−CN7B−CT2−CT2, and CN7B−CT2−CT2−NH2 (see Supporting Information for atom types) were fixed at the values from structure **A**. Charge separation (zwitterion character) was maintained in this way in the constrained optimization of **C**. Partial charges (q_i, q_j) were calculated using the CHELPG protocol[28] of Gaussian03 at these optimized geometries.

Three terminal functional groups are present in the species in Figure 1: $-NH_2$ (**A**), $-NH_3^+$ (**B**), and $-NHCO_2^-$ (**C**). Force field parametrization efforts were split into two categories: parameters excluding functional group atoms and parameters including functional group atoms. In the former case, the FF parameters (bond, angle, and improper force constants, dihedral profile parameters, and Lennard-Jones constants) were taken directly from the work of Cadena et al.[17] for the 1-butyl-3-methylimidazolium cation (with the exception of certain dihedrals, described below). Cadena et al. used parameters directly from the CHARMM 27 force field[29] and found that the results for liquid-state properties were in reasonable agreement with experiment.

In the latter case, bond force constants were obtained directly from the force constant matrix calculated at the B3LYP/TZVP[26,30] level of theory and scaled appropriately on the basis of comparisons to experimental vibrational frequencies for related molecules.[31] Unique angle force constants were derived by doing a series of structural perturbations on smaller related molecules where the angles were incremented by −2 to 2°, followed by single-point energy calculations at the B3LYP/TZVP level. The

(23) Yu, G.; Zhang, S.; Zhou, G.; Liu, X.; Chen, X. *AIChE J.* **2007**, *53*, 3210–3221.
(24) (a) Xu, H.; Rudkevich, D. M. *Chem. Eur. J.* **2004**, *10*, 5432–5442. (b) Hampe, E. H.; Rudkevich, D. M. *Chem. Commun.* **2002**, 1450–1451. (c) Xu, H.; Hampe, E. M.; Rudkevich, D. M. *Chem. Commum.* **2003**, 2828–2829. (d) Xu, H.; Rudkevich, D. M. *Org. Lett.* **2005**, *7*, 3223–3226. (e) Xu, H.; Rudkevich, D. M. *J. Org. Chem.* **2004**, *69*, 8609–8617.
(25) Canongia Lopes, J. N.; Padua, A. A. H. *J. Phys. Chem. B* **2004**, *108*, 16893–16898.
(26) (a) Becke, A. D. *J. Chem. Phys.* **1993**, *98*, 5648–5652. (b) Becke, A. D. *J. Chem. Phys.* **1993**, *98*, 1372–1377. (c) Lee, C.; Yang, W.; Parr, R. G. *Phys. Rev. B* **1988**, *37*, 785–789. (d) Krishnan, R.; Binkley, J. S.; Seeger, R.; Pople, J. A. J. *Chem. Phys.* **1980**, *72*, 650–654. (e) Clark, T.; Chandrasekhar, J.; Spitznagel, G. W.; Schleyer, P. v. R. *J. Comput. Chem.* **1983**, *4*, 294–301.
(27) Frisch, M. J.; et al. *Gaussian 03*, Revision D.01; Gaussian, Inc.: Wallingford, CT, 2004.
(28) Breneman, C. M.; Wiberg, K. B. *J. Comput. Chem.* **1990**, *11*, 361–373.
(29) MacKerell, A. D.; Wiorkiewicz-Kuczera, J.; Karplus, M. *J. Am. Chem. Soc.* **1995**, *117*, 11946–11975.
(30) Godbout, N.; Salahub, D. R.; Andzelm, J.; Wimmer, E. *Can. J. Chem.* **1992**, *70*, 560–571.
(31) Johnson, R. D., III. NIST Computational Chemistry Comparison and Benchmark Database, NIST Standard Reference Database Number 101, Release 14, September 2006, http://srdata.nist.gov/cccbdb.

force constants were derived assuming a harmonic approximation and averaged. Lennard-Jones (LJ) parameters for the N and H atoms of the functional groups were taken from Morgantini and Kollman,[32] and those for C and O of species **C** were taken from the CHARMM 22 force field for acetic acid.[33]

The dihedrals profiles *X*−CN7B−CT2−*Y*, *X*−CT2−CT2−*Y*, *X*−CT2−NH2−*Y*, *X*−CT2−NH3−*Y*, and *X*−NH2−CC−*Y* were fit using a combined ab initio/molecular mechanics (AI/MM) approach. *X* and *Y* correspond to all possible terminal atoms for the central bonds denoted above and are dictated by the dihedral connections that are present in **A**, **B**, and **C**. It is noted that the dihedral *X*−CN7B−CT2−*Y* *excludes* functional group atoms, but the parameters were fit using the AI/MM approach. The approach entails a building-up procedure such that all unique *X*, *Y* combinations for a given central bond are assigned on the basis of dihedral analysis for chemically similar smaller molecules. Redundancies in the H−C−C−H and H−C−C−C dihedrals allowed their assignment based on analysis of C_2H_6 and C_3H_8 dihedrals only. For species **A**, CH_3NH_2, $C_2H_5NH_2$, and $C_3H_7NH_2$ were used. For species **B**, $CH_3NH_3^+$, $C_2H_5NH_3^+$, and $C_3H_7NH_3^+$ were used. For species **C**, $NH_2CO_2^-$, $CH_2NHCO_2^-$, and $C_2H_5NHCO_2^-$ were used.

Dihedral angle energy profiles were obtained by incrementally rotating (±10°) the angle under consideration through 180 or 360°, depending on the symmetry of the molecule. Geometry optimizations were performed at each step at the B3LYP/TZVP level of theory, allowing the entire molecule to relax except the dihedral under study. Additional constraints on intramolecular degrees of freedom were added when necessary to obtain an energetic profile representative of the dihedral angle under investigation. The B3LYP/TZVP energy profile was found to closely reproduce MP2/cc-pVTZ(-f) results for these small molecules. Since nonbonded interactions can contribute significantly to the MM dihedral energy profile, relaxed MM calculations were also performed at each step in the dihedral scan with the particular FF dihedral parameters set to zero, following the procedure of Canongia Lopes et al.[34] The MM energies were then subtracted from the AI energies to obtain energy contributions solely from the dihedral rotation. This profile was then fit using a cosine series, as in eq 4. It is noted that unique CHELPG charges were calculated at the B3LYP/6-311+G* level for each small molecule or ion denoted above and LJ parameters were used consistent with those used for species **A**, **B**, and **C**.

Simulation Details

Molecular dynamics simulations in the isothermal−isobaric (NPT) and canonical (NVT) ensembles were performed using the program NAMD.[35] Pressure was controlled using a modified Nosé-Hoover method employing Langevin dynamics to control fluctuations in the barostat. Pressure was maintained (1 bar for all simulations) using barostat oscillation time and damping factors of 1 ps. Constant temperature (298.15 K for all simulations) was maintained using Langevin dynamics, with a damping factor of 5 ps^{-1}. A multiple time step algorithm was used with a 1 fs inner time step. Nonbonded interactions and full electrostatics were evaluated every 2 and 4 inner time steps, respectively. A particle mesh Ewald sum was used for handling the electrostatics. Nonbonded interactions were truncated using a switching function with a cutoff distance of 12.0 Å and a switching onset distance of 10.0 Å. The pair list cutoff distance was set to 14.0 Å. Intramolecular LJ and Coulombic interactions between atoms separated by exactly three bonds (intramolecular 1,4-interactions) were scaled by 50%, while interactions between fewer than three bonds were neglected. Atoms separated by three or more bonds were allowed to fully interact.

Table 1. Compositions and Number of Species Simulated

composition **A**:**B**:**C**	no. of species **A**	**B**	**C**	Tf_2N^-	x_{CO_2}[a]
1:0:0	200	0	0	200	0.000
8:1:1	160	20	20	200	0.091
3:1:1	120	40	40	200	0.167
2:1:1	100	50	50	200	0.200
1:1:1	67	67	67	201	0.250
1:2:2	40	80	80	200	0.286
0:1:1	0	100	100	200	0.333

[a] Equivalent mole fraction CO_2.

Simulations were performed to study various mixture compositions (**A**:**B**:**C**) to mimic the reaction of CO_2 with the TSIL, from partially to fully reacted. Table 1 includes the ratios that were studied, including the exact number of species in each case, as well as the mole fraction of CO_2 represented by each ratio. Only chemical complexation, not physical CO_2 absorption, was studied. Previous studies have shown that properties such as liquid density and the liquid structure are minimally affected by moderate amounts of physically absorbed CO_2.[20] The reaction being studied is shown in Scheme 1.

In Table 1, **A**:**B**:**C** represents the ratio of the number of product species formed (**B** and **C**) to the amount of unreacted TSIL (**A**). The anion (Tf_2N^-) is omitted from this ratio and is included for charge balance. For example, the 1:0:0 ratio represents pure TSIL, 2:1:1 represents half-reacted TSIL, and 0:1:1 represents fully reacted TSIL. The reacted species were chosen on the basis of the conclusions of Bates et al.[21] and the single-step mechanism proposed by Crooks and Donnellan;[11] i.e., no intermediate zwitterion species were considered. In addition to the compositions indicated in Table 1, the same compositions were studied containing ∼3.4 and ∼6.5 wt % water using the Simple Point Charge (SPC) water model,[36] corresponding to 164 and 328 water molecules, respectively.

For all systems, initial configurations were generated by randomly placing the appropriate number of molecules in a cubic simulation box. Equilibration of the dry systems was first performed in the NPT ensemble at elevated temperature (473 K) for 1.5 ns, followed by a quench to 298K and then an additional 5 ns simulation, resulting in converged densities in all cases. For the wet systems, the systems were simply equilibrated at 298 K for 5 ns. NVT simulations of 3 ns were then performed for all systems at the final average densities. To test the dependence of calculated properties on the procedure used to generate initial conditions, the above approach was also performed for the dry 8:1:1 and 0:1:1 systems using different initial random configurations and different quenching protocols (starting at 473 and 700 K). Hu and Margulis have noted that exploring various initial configurations is critical, particularly for systems characterized by distinct heterogeneity and local persistent environments, such as certain ionic liquids.[37]

Results and Discussion

A. Macroscopic Liquid Properties. Liquid Density and Molar Volume. The calculated liquid densities and molar

(32) Morgantini, P.-Y.; Kollman, P. A. *J. Am. Chem. Soc.* **1995**, *117*, 6057–6063.
(33) (a) Foloppe, N.; MacKerell, A. D., Jr. *J. Comput. Chem.* **2000**, *21*, 86–104. (b) MacKerell, A. D., Jr.; Banavali, N. *J. Comput. Chem.* **2000**, *21*, 105–120.
(34) Canongia Lopes, J. N.; Deschamps, J.; Padua, A. A. H. *J. Phys. Chem. B* **2004**, *108*, 2038–2047.
(35) Kale, L.; Skeel, R.; Bhandarkar, M.; Brunner, R.; Gursoy, A.; Krawetz, N.; Philips, J.; Shinozaki, A.; Varadarajan, K.; Schulten, K. *J. Comput. Chem.* **1999**, *151*, 283–312.
(36) Berendsen, H. J. C.; Postma, J. P. M.; van Gunsteren, W. F.; Hermans, J. *Intermolecular Forces*; D. Reidel, Dordrecht, The Netherlands, 1981.

Scheme 1. Proposed Stoichiometric Reaction of CO_2 with TSIL

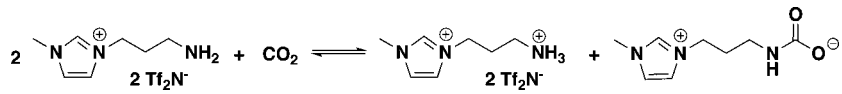

Table 2. Liquid Densities (g/cm^3), Molar Volumes (cm^3/mol), and Excess Molar Volumes (cm^3/mol) for Different Compositions

	no H_2O		164 H_2O			328 H_2O		
composition **A**:**B**:**C**	ρ	V_M	ρ	V_M	V_M^{ex}	ρ	V_M	V_M^{ex}
1:0:0[a]	1.556	270.1	1.531	156.2	−0.4	1.507	113.1	−0.4
8:1:1	1.562	272.0	1.540	156.8	−0.8	1.518	113.4	−0.9
3:1:1	1.568	273.7	1.556	156.7	−1.8	1.525	113.9	−1.0
2:1:1	1.574	274.1	1.557	157.5	−1.3	1.536	113.7	−1.3
1:1:1	1.578	275.7	1.563	158.9	−1.1	1.541	114.7	−1.2
1:2:2	1.579	277.3	1.564	159.0	−1.5	1.552	114.1	−2.1
0:1:1	1.586	278.9	1.574	159.6	−1.7	1.559	114.7	−2.2

[a] Experimental density at 298 K is 1.592 g/cm^3.[38]

volumes of the dry TSIL mixtures, as well as the mixtures containing 164 (∼3.4 wt %) and 328 (∼6.5 wt %) water molecules, are shown in Table 2. The number of water molecules included in the simulation was chosen to represent partially saturated systems based on preliminary experimental estimations.[38] From previous experimental and computational studies, the presence of water in ILs is known to significantly alter their physical and dynamical properties.[39,40] The density of the pure TSIL (1:0:0) was calculated to be 1.556 g/cm^3 from an equilibrated NPT simulation. This is in excellent agreement with the experimentally determined density of 1.592 g/cm^3, a difference of 2.26%.[38] The difference between computed and experimental density is consistent with what is typically observed for other IL force fields.[25] The corresponding calculated and experimental molar volumes for the pure TSIL are 270.1 and 264.0 cm^3/mol, respectively. If the amine group ($-NH_2$) of the TSIL is substituted with a methyl group ($-CH_3$), the resultant ionic liquid is 1-butyl-3-methylimidazolium bis-(trifluoromethanesulfonyl)imide ([Bmim][Tf_2N]), a non-TSIL analogue of [**A**][Tf_2N]. The experimental liquid density and molar volume of [Bmim][Tf_2N] are 1.437 and 291.8 cm^3/mol, respectively.[16] Thus, replacement of the $-CH_3$ group with an $-NH_2$ group results in a substantial increase in the density by nearly 10% (with respect to the experimental value) and a dramatic lowering of the molar volume by ∼30 cm^3/mol. This alone suggests there is less free volume in the TSIL, which is at least partially responsible for the increase in viscosity of the TSIL compared to the unfunctionalized IL. Previous studies have indicated that a simple model based primarily on molar volume can be used to reliably predict gas solubilities in imidazolium-based ionic liquids.[41] For a particular gas, solubility is predicted to increase with increasing molar volume. Here it is predicted that CO_2 *physical* solubility should be somewhat less in the [**A**][Tf_2N] TSIL than in the non-TSIL analogue, [Bmim][Tf_2N].

As the mole fraction of reacted CO_2 increases in the dry TSIL, the calculated density increases linearly from 1.562 to 1.586 g/cm^3, a total increase of ∼2% relative to the pure TSIL. The molar volumes also exhibit an increasing trend over the composition range, initially increasing to 272 cm^3/mol and ranging up to 278.9 cm^3/mol for the fully reacted system. This suggests that physical CO_2 solubility should also increase slightly in this range. Based on solubility vs molar volume correlations, it likely that the Henry's constant for physical CO_2 absorption in this TSIL will be higher than that for [Bmim][Tf_2N] of 59.0 bar.[16] In the mixtures spanning 8:1:1 to 0:1:1, no physically dissolved CO_2 was considered in the simulations. Moderate amounts of physically dissolved CO_2 have been shown to result in little to no expansion of the liquid phase in [Bmim][PF_6],[42] likely due to occupying free cavity volume within the liquid,[20] and therefore it seems reasonable that neglect of physically dissolved CO_2 will not have a dramatic effect on the results described herein.

The simulated physical properties of the pure TSIL (1:0:0) and the mixtures (8:1:1 to 0:1:1) are observed to vary according to water content. As shown in Table 2, the simulation mixtures containing 164 water molecules (∼3.4 wt %) have lower densities compared to the dry counterparts, ranging from 1.6% lower for the 1:0:0 case and decreasing to 0.75% lower for the fully reacted 0:1:1 system. The molar volumes of the mixtures (including moles of H_2O) also increase from 156.2 to 159.6 cm^3/mol over this span, an increase of 2.2%. The excess molar volumes have also been calculated and are shown in Table 2. The excess molar volumes are all negative, but small in magnitude, indicating that the molar density is only slightly higher than what would be expected of a system having ideal mixing.

The simulation mixtures containing 328 water molecules (∼6.5 wt %) follow a similar trend. Addition of water to the dry 1:0:0 system results in a 3.1% decrease in the density to 1.507 g/cm^3. The densities decrease for the remaining systems as well, although the percent decrease drops off gradually, with the decrease in the 0:1:1 system being only 1.7% with a value of 1.559 g/cm^3. The molar volumes also show a small increase over the composition range going from 113.1 to 114.7 cm^3/mol, an increase of only 1.4%. Once again, the excess molar volumes are negative and of similar magnitude with respect to the 164 water molecule system, indicating relatively minor deviations from ideal mixing.

Mean-Squared Displacement and Rotational Relaxation. The dynamic nature of the pure TSIL (1:0:0) and its reacted mixtures (8:1:1 to 0:1:1) was characterized by studying the center-of-mass (COM) mean-squared displacements (MSDs) of **A**, **B**, **C**, Tf_2N^-, and H_2O as a function of time. It is well established that the self-diffusion coefficient for a fluid, or in the case of an IL the cation or anion, can be calculated using the Einstein relation,[43]

$$D_s = \frac{1}{6}\lim_{t\to\infty}\frac{d}{dt}\langle|\vec{r}(t)-\vec{r}(0)|^2\rangle \qquad (5)$$

where the bracketed quantity represents the MSD. It has been shown previously that it is critical that the system exhibit true

(37) Hu, Z.; Margulis, C. J. *Proc. Natl. Acad. Sci. U.S.A.* **2006**, *103*, 831–836.
(38) Brennecke, J. F., personal communication.
(39) Anthony, J. L.; Maginn, E. J.; Brennecke, J. F. *J. Phys. Chem. B* **2001**, *105*, 10942–10949.
(40) Kelkar, M. S.; Maginn, E. J. *J. Phys. Chem. B* **2007**, *111*, 4867–4876.
(41) Camper, D.; Bara, J.; Koval, C.; Noble, R. *Ind. Eng. Chem. Res.* **2006**, *45*, 6279–6283.
(42) Blanchard, L. A.; Hancu, D.; Beckman, E. J.; Brennecke, J. F. *Nature* **1999**, *399*, 28–29.
(43) Frenkel, D.; Smit, B. *Understanding Molecular Simulation*; Academic Press: New York, 1996.

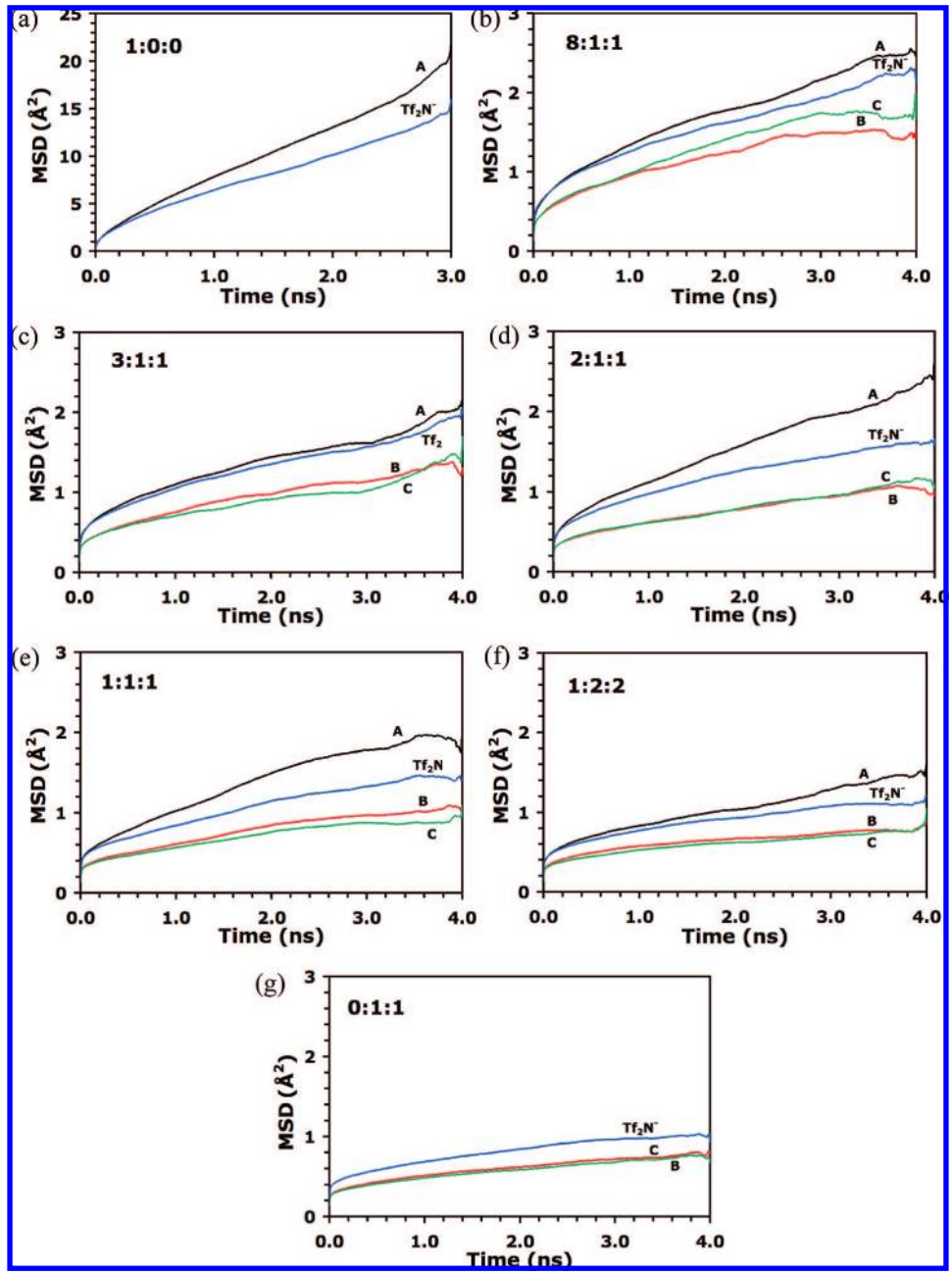

Figure 2. Mean-square displacements (Å^2) vs time (ns) at different dry system compositions: (a) 0:1:1, (b) 8:1:1, (c) 3:1:1, (d) 2:1:1, (e) 1:1:1, (f) 1:2:2, and (g) 0:1:1.

diffusive motion, particularly in the case of ILs that tend to have sluggish dynamics, prohibiting adequate sampling at sufficient time lengths.[44] Subdiffusive behavior can be identified by $\beta < 1$ calculated from the following expression:

$$\beta(t) = \frac{\mathrm{d}(\log(\Delta r^2))}{\mathrm{d}(\log(t))} \qquad (6)$$

where Δr^2 is the COM MSD over time t. Figure 2 contains plots of total COM MSD versus time for the components of dry systems 1:0:0 through 0:1:1. Total COM MSD values are the sum of the individual x, y, and z COM MSD contributions. Several key features relevant to the nature of the dynamics of the pure and reacted TSIL systems may be deduced simply from the behavior demonstrated in Figure 2. At immediate glance, Figure 2 shows characteristic behavior for MSD vs time, with a sharp rise at very short times, characteristic of ballistic motion, followed by an increase of apparently constant slope over the course of the simulation. From Figure 2a, it is apparent that the cation (**A**) and anion (Tf_2N^-) display independent dynamics, with the cation showing higher MSDs than the anion over time. A plot of $\beta(t)$ (not shown) clearly indicates $\beta < 1$ over the time interval of interest and suggests nondiffusive behavior. Much longer simulations would be required to quantitatively study true self-diffusive behavior, and thus only behavior that is *apparent* from the current simulations may be discussed.

Figures 2b−g for the reacted mixtures show astonishing behavior relative to the pure case. Immediately, at the lowest

(44) (a) Cadena, C.; Maginn, E. J. *J. Phys. Chem. B* **2006**, *110*, 18026–18039. (b) Cadena, C.; Zhao, Q.; Snurr, R. Q.; Maginn, E. J. *J. Phys. Chem. B* **2006**, *110*, 2821–2832.

equivalent mole fraction of CO_2 (8:1:1 system), there is a precipitous drop of nearly an order of magnitude in the MSDs of the cation (**A**) and the anion (Tf_2N^-) over time. However, the relative ordering remains the same, with the cation showing higher MSDs than the anion beyond 1 ns. A major difference in 8:1:1 relative to 1:0:0 is the presence of the quaternary ammonium (**B**) and carbamate species (**C**). The MSDs of **B** and **C** over time are of similar magnitude (slightly higher for **C**) yet are noticeably lower than those of **A** and Tf_2N^-. It may be initially concluded, therefore, that the immediate introduction of a small amount of CO_2 to the TSIL system, causing a chemical reaction and formation of **B** and **C** species, results in a dramatic slowing of the dynamics of the system. This is entirely consistent with the experimentally observed increase in viscosity upon introduction of CO_2.

Introduction of more CO_2 into the system, represented by composition 3:1:1, causes the MSDs vs time of all four species to fall off relative to the 8:1:1, further dampening the dynamics of the system. Again, the MSDs of **A** and Tf_2N^- are higher than those of **B** and **C**, indicating greater diffusive motion of the former two species relative to the latter two. However, the MSDs of **B** and **C** are now nearly identical over the course of the simulation. This *suggests*, without further information regarding the microscopic organization of the liquid structure, that there is an important interaction between the **B** and **C** species in the system.

As the amount of complexed CO_2 increases on going from 2:1:1 to 0:1:1, the dynamics of the system become continually more sluggish, indicated by recurrent drops in the MSDs of all system components. In fact, at the 1:2:2 and 0:1:1 compositions, the MSDs for all components are almost entirely below 1.5 and 1 $Å^2$, respectively, over the 4 ns simulation, indicating that the COMs of these species are practically static. The MSDs of **A** (except 0:1:1, where **A** is absent) and Tf_2N^- are always greater than the **B** and **C** components, although they are not necessarily closely correlated. For example, in system 3:1:1, the behavior of **A** and Tf_2N^- appears to be closely correlated, yet this correlation disappears in systems 2:1:1 and 1:1:1, which show behavior reminiscent of the pure system. This may be attributed to several reasons, including inherent inhomogeneity of the equilibrated systems or weaker, fluctuating interactions between **A** and Tf_2N^- relative to **B** and **C**. The MSDs versus time for **B** and **C** over the compositions 2:1:1 to 0:1:1 remain tightly correlated, and the curves nearly overlay in all cases. This is again suggestive of a strong 1:1 interaction between these two species.

Addition of water to the pure TSIL and to its mixtures (8:1:1 to 0:1:1) significantly changes the dynamics of the systems. The MSDs versus time of **A**, **B**, **C**, and Tf_2N^- for the different compositions containing H_2O are shown in Figure 3. Each component is plotted and differentiated according to the number of water molecules in the system, 164 or 328. Upon addition of 164 water molecules, the MSDs of **A** and Tf_2N^-, and hence the dynamics, in the pure system (Figure 3a) fall off significantly after 3 ns when compared to the dry system (Figure 2a). By diluting the system with water, the dynamics of the system would be expected to increase. Instead, what is observed is that the dynamics initially drop off, before increasing with higher concentrations of water. This counter-intuitive observation at low water concentrations is due to the formation of hydrogen bond "bridges" between water and neighboring **A** and Tf_2N^- species.[45] Upon addition or more water to the system (328 molecules), the MSDs of the pure components increase relative to the low H_2O concentration case, likely due to a dilution effect caused by increased probability of H_2O-H_2O interactions.

In the mixtures, illustrated in Figure 3b−g, the dynamics follow the expected trend. The addition of 164 and 328 water molecules causes the dynamics to speed up in all cases. The MSDs vs time for all component species are larger relative to those in the corresponding dry systems, and the MSDs vs time in the systems containing 328 H_2O molecules are larger than those in the analogous 164 H_2O molecules systems. In the 8:1:1 system, all of the MSD vs time curves are separated. This is consistent with the dry 8:1:1 system results; all COM displacements are uncorrelated. However, at higher CO_2 concentrations, represented by 3:1:1 and beyond, the translational dynamics of **B** and **C** are strongly correlated, consistent with what was observed in the analogous dry systems, while the translational dynamics of **A** and Tf_2N^- are essentially independent of one another. Thus, the presence of water does little to disrupt the strong interaction between **B** and **C**, despite the speed-up in dynamics of the two species. Water does little to affect the relative MSD difference between **A** and Tf_2N^-; it speeds up the dynamics of both at all compositions except 1:0:0.

Self-diffusion coefficients (D_s) were estimated for both the dry and wet systems using the Einstein relation of eq 5. At very long times, there is significant noise due to poor statistics, and therefore analysis is performed at an intermediate time interval (i.e., 1−2 ns for 1:0:0 and 1−3 ns for all others). As mentioned above, **A** and Tf_2N^- for the dry 1:0:0 system both had characteristic $\beta < 1$ over the course of the simulation, indicative of subdiffusive behavior. In addition, this system was found to have the fastest dynamics of all those studied, as shown in Figure 2a relative to all other figures. Thus, it can be stated with confidence that the species in all of the remaining systems possess subdiffusive behavior as well over the duration of the simulations. The self-diffusion coefficients presented in Table 3 are thus "apparent" or estimated D_s values (with high standard deviations) but should not be confused with the true self-diffusivities that could only be computed with intractably long simulations. Apparent self-diffusivities were computed because they enable important qualitative trends to be elucidated from the data.

In the dry systems, the self-diffusion coefficients for the species in the 1:0:0 system are an order of magnitude larger than those in the remaining dry systems (8:1:1 to 0:1:1). Although some fluctuation exists, there is a definite decreasing trend on going from 8:1:1 to 0:1:1. Systems 8:1:1 to 1:1:1 have apparent D_s values in the range of $3 \times 10^{-13}-7 \times 10^{-13}$ m^2/s, while the remaining systems 1:2:2 and 0:1:1 are in the range of $1 \times 10^{-13}-4 \times 10^{-13}$ m^2/s. These estimated D_s values for the reacted systems are an order of magnitude smaller than those calculated for some other traditional IL systems.[44]

To test the dependence of the computed dynamic properties on the initial system configurations, several initial conditions were tried for the dry 8:1:1 and 0:1:1 systems. In addition to the simulations described in the Simulation Details, two new random configurations were generated for each composition with NPT equilibrations at 473 or 700 K, followed by quenching and NPT equilibration at 298 K. The results of these simulations are provided in the Supporting Information, Figure S3 (MSD vs time) and Table S7 (self-diffusion coefficients). These results indicate that the absolute calculated dynamic values are con-

(45) Kelkar, M.; Shi, W.; Maginn, E. J. *Ind. Eng. Chem. Res.*, published online Sep 9, 2008 http://dx.doi.org/10.1021/ie800843u.

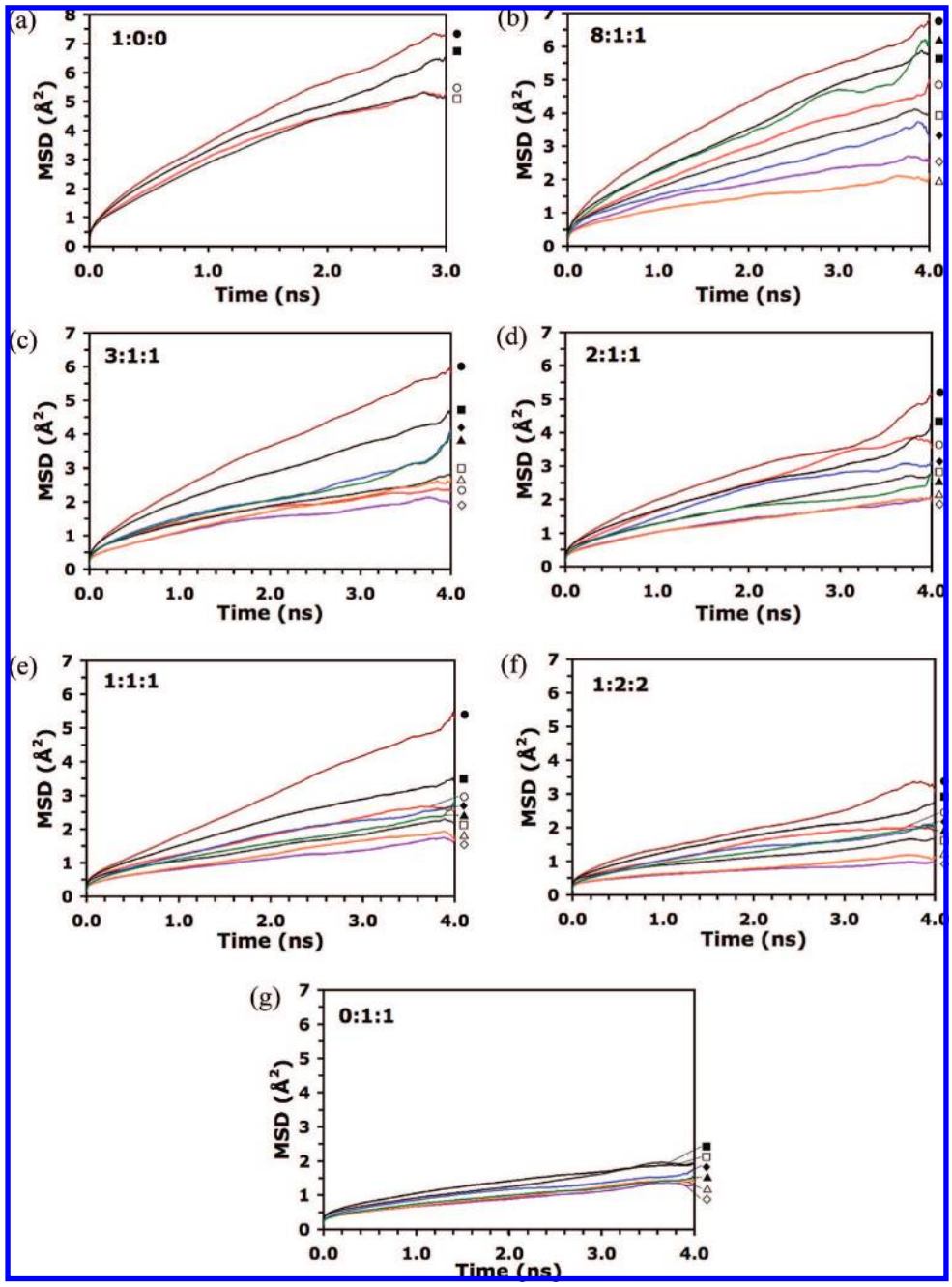

Figure 3. Mean-square displacements (Å^2) vs time (ns) at different wet system compositions (excluding H_2O MSDs): (a) 0:1:1, (b) 8:1:1, (c) 3:1:1, (d) 2:1:1, (e) 1:1:1, (f) 1:2:2, and (g) 0:1:1. Filled and open symbols represent 328 and 164 H_2O systems, respectively, with **A** (●,○), **B** (◆,◇), **C** (▲,△), and Tf_2N^- (■,□) labeled.

figuration dependent, due to the formation of heterogeneous, persistent local environments as described by Hu and Margulis for ILs;[37] however, the values do have large error bars. Thus, in addition to limitations due to slow dynamics, these heterogeneities prevent quantitative analysis of the system dynamics on the simulation time scale. Nonetheless, a dramatic, systematic decrease in the system dynamics upon CO_2 complexation is still unequivocally supported by the results.

The D_s values of **A** and Tf_2N^- in the wet 1:0:0 system fall of by a factor of ∼3.5 and ∼2.5, respectively, in the 164 H_2O system, and by ∼2.5 for both in the 328 H_2O system. In the remaining mixtures (8:1:1 to 0:1:1), the D_s values for **A**, **B**, **C**, and Tf_2N^- increase with increasing H_2O content. In the 164 H_2O system, the average increase in D_s is ∼2.0 times relative to the dry case, while in the 328 H_2O system the average increase is ∼3.5 times.

The dynamics of the H_2O molecules themselves also exhibit interesting behavior. Table 3 contains D_s values for the H_2O molecules in each system. For any given system composition, the D_s values for H_2O increase with increasing water content, by about a factor of 2, as would be expected. However, with increasing equivalent CO_2 mole fraction, the D_s values drop off dramatically. From 1:0:0 to 0:1:1, there is a factor of 10 and 5 decrease in D_s for the 164 and 328 H_2O systems, respectively. This is also graphically illustrated in Figure 4, where the slopes of the MSD vs time curves decrease with increasing CO_2 mole fraction. This is due to the presence of bound versus unbound water, the former increasing as the

Table 3. Apparent[a] Self-Diffusion Coefficients ($\times 10^{13}$ m^2/s) with Standard Deviations vs System Composition

		no H_2O		164 H_2O		328 H_2O	
composition **A**:**B**:**C**[b]	species	D_s	$\pm\sigma$	D_s	$\pm\sigma$	D_s	$\pm\sigma_{Ds}$
1:0:0	**A**	86.5	6.0	23.6	6.0	35.2	5.5
	Tf_2N^-	62.0	8.5	27.2	3.4	26.5	5.2
	H_2O	–	–	328.0	19.1	433.4	37.7
8:1:1	**A**	6.9	2.0	16.8	2.9	22.1	3.8
	B	4.5	2.8	8.1	2.7	11.7	3.5
	C	6.4	1.9	5.5	2.8	20.5	5.7
	Tf_2N^-	5.6	1.6	13.9	1.8	21.6	2.6
	H_2O	–	–	142.9	8.4	303.2	23.0
3:1:1	**A**	4.4	1.8	6.1	3.0	20.3	3.1
	B	3.2	1.9	5.9	3.0	9.8	3.7
	C	2.6	1.7	8.5	2.2	9.1	2.7
	Tf_2N^-	4.4	1.4	7.7	1.7	14.2	2.2
	H_2O	–	–	92.8	16.0	214.1	17.1
2:1:1	**A**	7.2	1.8	14.3	2.2	12.8	3.6
	B	2.8	1.0	5.9	1.6	11.2	4.5
	C	2.9	1.1	5.8	1.3	6.0	3.4
	Tf_2N^-	4.1	1.3	8.4	1.2	10.8	2.6
	H_2O	–	–	80.6	17.8	139.5	17.5
1:1:1	**A**	6.4	2.1	9.3	1.8	19.8	2.5
	B	3.0	1.2	4.7	1.5	8.8	2.6
	C	2.6	1.0	6.7	1.3	7.3	1.4
	Tf_2N^-	4.1	1.4	6.5	1.5	11.6	1.9
	H_2O	–	–	52.9	7.9	135.2	13.9
1:2:2	**A**	3.8	1.6	7.5	2.6	9.3	1.9
	B	1.3	0.8	2.0	0.9	4.8	2.4
	C	1.5	0.7	3.1	1.0	5.9	1.1
	Tf_2N^-	2.6	1.0	3.8	0.9	7.3	1.8
	H_2O	–	–	39.3	5.4	73.3	7.2
0:1:1	**B**	1.7	0.6	3.6	0.7	4.2	1.5
	C	1.6	0.5	4.6	0.9	3.8	0.9
	Tf_2N^-	2.3	0.8	5.8	0.9	5.3	1.3
	H_2O	–	–	29.7	4.5	82.6	5.6

[a] Estimated due to very slow dynamics. [b] Calculated over 1−2 ns interval for 1:0:0 systems and 1−3 ns interval for all other systems.

number of **B** and **C** species increases, suggesting a strong electrostatic interaction with the charged carbamate and quaternary ammonium tails.

As an additional metric of system dynamics, the rotational time constant was calculated for each species. The rotational dynamics of the individual **A**, **B**, **C**, Tf_2N^-, and H_2O species can be studied using the following correlation function:

$$C(t) = \left\langle \frac{1}{2}[3\cos^2\theta_i(t) - 1] \right\rangle \tag{7}$$

where $\theta_i(t)$ is the angle of a vector formed between itself at time t and the original vector time $t = 0$. $C(t)$ will decay to zero as the molecule loses orientational correlation.[46] The rotational correlation time constant, τ, was computed for each species by assigning the vector in eq 7 to the longest principal axis of the species and using the following relation:

$$\tau = \int_0^\infty C(t)\,\mathrm{d}t \tag{8}$$

where $c(t)$ was fit to a stretched exponential of the form

$$C(t) = a_0\, \mathrm{e}^{-(t/\tau_0)^\beta} \tag{9}$$

where a_0 is a constant, τ_0 is the rotational time constant at $t = 0$, and β is a stretching parameter that varies between 0 and 1 (not to be confused with β from eq 6). Materials with β values significantly below unity are indicative of glasses and exhibit slow rotational relaxation and dynamics.[47]

Table 4 contains rotational time constants for systems 1:0:0, 8:1:1, and 0:1:1, with and without water. Significant difficulties were encountered in fitting stretched exponentials to the rotational correlation data, particularly for the CO_2-reacted systems. As demonstrated earlier, these systems have very small COM MSDs over long time intervals, and hence very slow translational dynamics. Very slow rotational dynamics are also observed for the systems containing CO_2. The example plots in Figure 5 illustrate how $C(t)$ varies with time for various species in different mixtures, as well as the resultant stretched exponential fits. Figure 5a contains a well-behaved rotational correlation function decay curve, observed for species **A** in the dry 1:0:0 TSIL system. The rotational time constants for **A** and Tf_2N^- in dry 1:0:0 are about 1.5 and 1.0 ns, respectively, as shown in Table 4. Addition of 164 H_2O molecules causes the rotational time constants to increase to 4.9 and 3.7 ns, respectively, followed by a decrease to 3.7 and 2.4 ns with 328 water molecules. This is consistent with the MSD vs time behavior observed for the same system.

A tremendous increase is observed for the rotational time constants for the 8:1:1 system. In the dry system, τ for **A** and Tf_2N^- increases by nearly a factor of 50, followed by significant decreases with the addition of water. Even more astonishing, however, are the τ values for **B** and **C**, which are on the order of hundreds of nanoseconds in the dry system. Addition of water molecules also causes these τ values to fall off significantly, resulting in τ values in the tens of nanoseconds. Thus, it is now evident that simulations of only a few nanoseconds (such as those done in this study) are entirely inadequate to properly sample sufficiently long time scales to quantitatively evaluate the rotational time constants for the reacted systems. This is even more evident in Figure 5b. Over the course of 4 ns, the correlation curve tails off only to about 0.85 to 0.90 and has significant noise, due to the very sluggish dynamics and inadequate sampling and statistics.

Data for the fully reacted case (0:1:1) are also provided in Table 4. In the dry system, τ values obtained from the best attempt to fit eq 9 for **B**, **C**, and Tf_2N^- are on the order of *thousands* of nanoseconds. For this system, essentially no rotational motion is observed over the entire duration of the simulation. Addition of water to the system has only a slight dampening effect, and τ values are still incredibly long, on the order of tens to hundreds of nanoseconds. Figure 5c illustrates the difficulty and unreliability in fitting the data in this case, where $C(t)$ decreases to merely 0.95 over the 4 ns simulation. Data have not been provided for systems 3:1:1 to 1:2:2, as the results are unreliable due to the slow rotational dynamics. However, from a semiquantitative perspective, the rotational time constants provide further evidence of the extremely slow dynamics of the system. It would be entirely intractable to simulate for long enough periods of time to adequately sample these systems.

For the 1:0:0 system (dry and wet), the β value from eq 9 falls in the range of 0.65−0.75. In the dry 8:1:1 and 0:1:1

(46) McQuarrie, D. A. *Statistical Mechanics*; University Science Books: Sausalito, CA, 2000.

(47) Phillips, J. C. *Rep. Prog. Phys.* **1996**, *59*, 1133–1207.

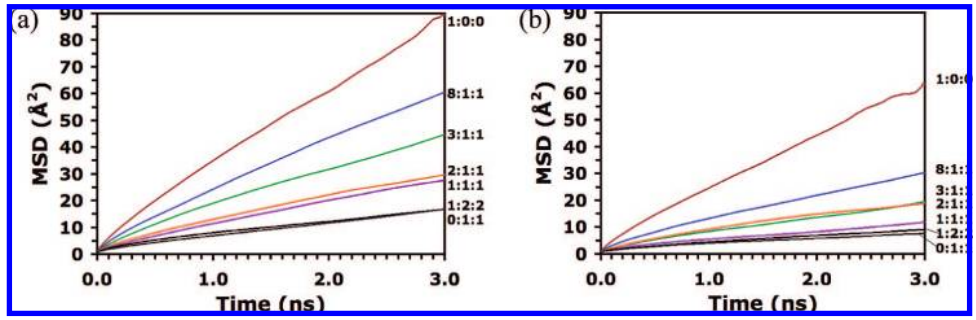

Figure 4. Mean square displacements (Å^2) vs time (ns) of H_2O molecules at different wet system compositions and water contents: (a) 328 H_2O and (b) 164 H_2O.

Table 4. Estimated Rotational Time Constants (ns) for Longest Molecular Axis for Selected System Compositions

			rotational time constant (τ)		
equiv mole fraction CO_2	composition **A**:**B**:**C**	species	dry	164 H_2O	328 H_2O
0.000(none)	1:0:0	**A**	1.5	4.9	3.7
		Tf_2N^-	1.1	3.7	2.4
		H_2O	−	0.2	0.2
0.091 (min)	8:1:1	**A**	50.3	9.6	8.0
		B	130.5	39.7	14.8
		C	450.1	54.3	17.7
		Tf_2N^-	47.5	8.1	4.1
		H_2O	−	0.5	0.3
0.333 (max)	0:1:1	**B**	1112.7	145.7	148.9
		C	4315.4	281.1	248.2
		Tf_2N^-	1206.7	55.5	38.6
		H_2O	−	5.1	4.0

systems, however, β values fall in the range of 0.4−0.6, which is typical of glassy dynamics. When combined with the dramatic increase in τ and reductions in the MSDs upon formation of the dication (**B**) and zwitterion (**C**) species, these results are entirely consistent with the experimental observations[22] that the introduction of CO_2 to the amine-functionalized TSIL causes a rapid and dramatic slowing of the dynamics, which manifests itself in a sharp increase in viscosity. The simulations predict that the addition of water will speed the dynamics relative to the dry case, but the system will still exhibit sluggish dynamics relative to conventional solvents.

B. Microscopic Liquid Properties. Hydrogen Bonding in the Liquid. In order to understand the microscopic interactions that underlie the macroscopic dynamical properties described above, a detailed hydrogen bond analysis in the liquid was performed. Hydrogen bond criteria were established according to Scheme 2, where D is the donor atom, A is the acceptor atom, r_H is the donor−acceptor distance, and θ_H is the angle formed by D−H···A. The hash-marked line represents hydrogen bonding. The cutoff for the r_H distance was chosen as <3.3 Å, and the cutoff for the θ_H angle was chosen as >145°. This is consistent with hydrogen bonds for small molecules in general,[48] and in particular for what has been observed for ionic liquids in the solid state.[49] Hydrogen bonds that met both criteria were counted on a per snapshot/trajectory basis over the course of each NVT simulation and averaged. All possible hydrogen bond donors were considered, particularly known interaction loci, including all nitrogen donor sites in **A** (−NH_2), **B** (−NH_3), and **C** (>NH) with bound hydrogen atoms, the C2, C4, and C5 positions in the imidazolium ring (−CH) with bound hydrogen atoms, and the typical water donor sites (OH_2). Acceptor sites include the oxygen, fluorine, and nitrogen sites in the Tf_2N^- anion, the terminal carbamate oxygen atoms in **C**, and the typical oxygen acceptor of H_2O. These sites are differentiated in Tables 5 (dry) and 6 (wet). The absolute number of hydrogen bonds counted has little importance, as the number of species changes with increasing equivalent CO_2 mole fraction. Thus, the relative importance of each hydrogen bond type was determined by counting the total number possible in the liquid at a given composition, assuming a 1:1 saturation value, and determining the fraction or percentage of those particular interactions that occur or that are "occupied" in the simulation. Thus, it is possible to quantify the appearance or disappearance of a particular type of hydrogen bond on the basis of its fractional "occupancy". Based on these importance criteria, the fraction of sites occupied for a particular donor or acceptor should sum to one over all interactions if fully occupied. However, this is rarely the case because not all sites will be occupied due to steric constraints, the inherent disorder in the liquid state, or failure to meet the acceptance criteria of Scheme 2. Also, fractional occupancies of greater than one are possible if the saturation ratio of 1:1 is violated, i.e., if bifurcated hydrogen bonds exist in the liquid. Bifurcated hydrogen bonds are most probable for interactions involving the H_2O molecule due to its compact size and ability to share spatial volume more effectively than the bulkier TSIL species. Periodic boundary conditions were not accounted for during the counting, and thus the number of hydrogen bonds is likely slightly underestimated.

Table 5 shows the percentage of hydrogen bonds occupied of a given type as a function of dry system composition. Although a much larger number of hydrogen bond types were counted, only those that had 10% occupancy or greater are listed. For example, it was found that hydrogen bonding involving the C4 and C5 positions of the imidazolium ring or the F and N sites of the Tf_2N^- anion has relatively little importance, and hence those contributions were omitted. As shown in Table 5, interactions between the C2 position (donor) of the ring (>CH) and oxygen acceptors on **C** and Tf_2N^- have a relatively small, but constant occupancy. It is noted that the interaction between >CH (donor) of **C** and −O (acceptor) of **C** constitutes both a neighboring interaction and a self-interaction in which the alkyl chain wraps around and interacts with the ring hydrogen (as noted above when discussing the force field development).

The most important interactions occur between the terminal nitrogen donor functionalities on **A**, **B**, and **C** (i.e., −NH_2, −NH_3, >NH) and the oxygen acceptors on **C** (denoted **A**···**C**,

(48) Grabowski, S. J. *Annu. Rep. Prog. Chem., Sect. C* **2006**, *102*, 131–165.
(49) Holbrey, J. D.; Reichert, W. M.; Rogers, R. D. *Dalton Trans.* **2004**, 2267–2271.

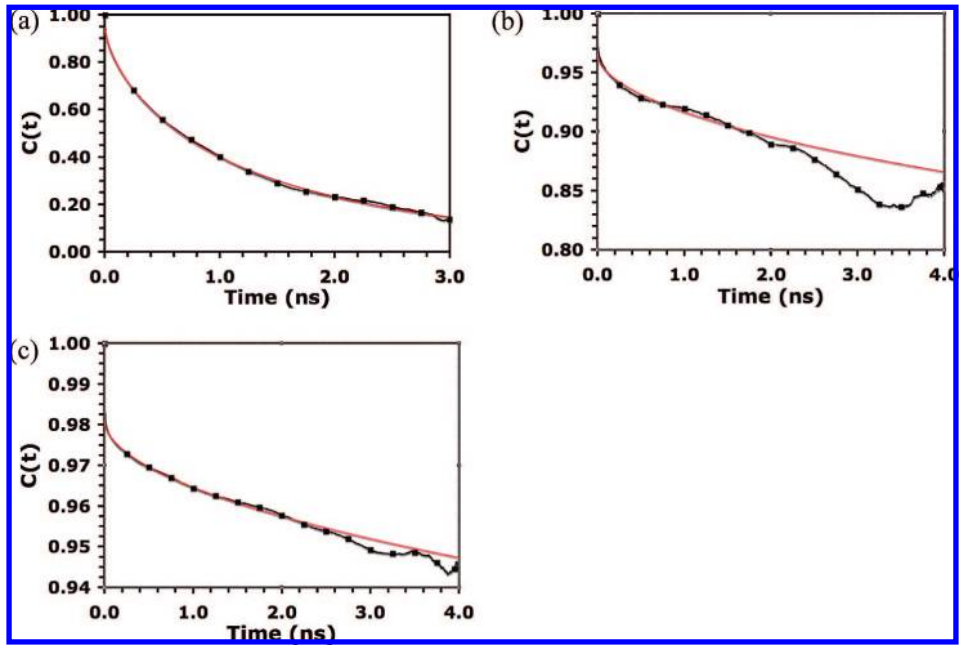

Figure 5. Longest principal axis rotational correlation raw data (■) and stretched exponential fits (solid) for selected species in different systems, illustrating good fit (1:0:0, Species **A**) (a), poor statistics and slow relaxation (8:1:1, Species **C**) (b), and extremely slow relaxation (0:1:1, Species **C**) (c).

Scheme 2. Hydrogen-Bonding Criteria

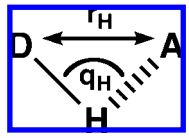

Table 5. Hydrogen Bond Analysis (% Occupied, by Type) vs System Composition (Dry)

D−H[a]	species	A[b]	species	1:0:0	8:1:1	3:1:1	2:1:1	1:1:1	1:2:2	0:1:1
$-NH_2$	**A**	−O	**C**	−	51.7	41.6	26.9	13.8	15.2	−
>CH	**A**	−O	**C**	−	16.4	10.6	8.0	7.1	14.8	−
$-NH_2$	**A**	−O	Tf_2N^-	25.1	24.4	19.4	22.3	25.6	21.5	−
>CH	**A**	−O	Tf_2N^-	14.4	12.1	10.8	10.6	10.8	7.2	−
$-NH_3$	**B**	−O	**C**	−	26.5	34.2	37.7	43.5	48.4	51.7
>CH	**B**	−O	**C**	−	3.9	4.9	8.7	5.4	5.7	9.3
$-NH_3$	**B**	−O	Tf_2N^-	−	27.5	23.9	22.1	19.3	17.0	19.3
>CH	**B**	−O	Tf_2N^-	−	13.6	10.5	8.9	8.5	10.7	8.9
>NH	**C**	−O	**C**	−	17.7	3.9	13.3	9.0	17.1	21.6
>CH	**C**	−O	**C**	−	13.9	19.9	26.0	15.4	17.0	25.1
>NH	**C**	−O	Tf_2N^-	−	20.0	23.8	18.5	15.9	14.4	12.8
−CH	**C**	−O	Tf_2N^-	−	13.4	11.6	8.5	10.1	11.4	8.6

[a] Donor site (with D = N or C). $-NH_2$, $-NH_3$, and >NH are amine donor sites of **A**, **B**, and **C** respectively. >CH is donor site at the C2 position of the imidazolium ring. [b] Acceptor site. −O is acceptor site of **C** or Tf_2N^-.

B···**C**, and **C**···**C**, respectively) and Tf_2N^-. These donor interactions with the Tf_2N^- are relatively constant at about 20−25%, due to the high probability of having a Tf_2N^- in the immediate vicinity. A previous simulation study has shown that the amine interactions with the anion in the pure (unreacted) imidazolium TSILs are the source of their unusually high viscosities relative to the non-TSIL analogues.[23] These interactions are illustrated from a simulation snapshot in Figure 6a,b. However, the **A**···**C** (Figure 6c) and **B**···**C** interactions reveal an enlightening trend. At low equivalent concentrations of CO_2, the fraction of these sites occupied in the former is 51.7% and in the latter is 26.5%. This is consistent with the larger number of **A** relative to **B** at low concentrations. However, as CO_2 concentrations increase, a larger number of **B**···**C** interactions become occupied relative to **A**···**C**, ultimately ending at 48.4% and 15.2%, respectively, at the 1:2:2 composition and 51.7% **B**···**C** in the fully reacted system (0:1:1). Once again, there is nothing telling here, as a larger number of **B** are present at higher concentrations of CO_2. However, piecing together the puzzle reveals the origin of the slow bulk dynamics, as discussed below.

Figures 7 and 8 show the radial pair distribution functions ($g(r)$ vs r) for **B**···**C** and **A**···**C** H···O interactions, respectively. The ammonium−carbamate hydrogen-bonding correlation for **B**···**C** (Figure 7) reveals a sharp, narrow peak at 1.85 Å for the N−H···O interaction, with a smaller peak at ∼3.3 Å due to close contacts with the remaining ammonium hydrogens. The amine−carbamate hydrogen-bonding correlation for **A**···**C** (Figure 8) between N−H···O is at a slightly longer distance of 1.95 Å, indicating a weaker interaction, with a similar small peak at ∼3.3 Å. Also informative is the intensity of the $g(r)$ peak at short distance. The peak heights for the **B**···**C** interaction are ∼3.5 times greater than those for the **A**···**C** interaction. This indicates that, relative to no interaction ($g(r) = 1$), there is much greater probability of observing the **B**···**C** interaction versus the **A**···**C** in the liquid at a given composition.

The reason for this enhanced probability is evident when considering the partial charges on the individual atoms of the $-NH_2$, $-NH_3^+$, and $-NHCO_2^-$ groups. There is a partial negative charge of −1.06 e on the amine nitrogen of **A** versus −0.52 e on the ammonium nitrogen of **B**, with other charges being comparable for terminal H and O atoms in the **A**, **B**, and **C** species. This points toward a hydrogen-bonding interaction between **B**···**C** that is much stronger than that between **A**···**C**. In fact, this is entirely consistent with the MSD vs time, D_s, and τ results discussed previously, where **B** and **C** were discovered to show correlated behavior in all cases and **A** and **C** were not correlated. Thus, as the equivalent CO_2 mole fraction increases, the liquids become inundated with persistent, strong hydrogen-bonded networks of $(\mathbf{B}\cdots\mathbf{C})_n$ chains or clusters (as illustrated in Figures 9a,b) that underlie the slow macroscopic dynamics observed experimentally and computationally. These

Table 6. Hydrogen Bond Analysis (% Occupied, by Type) vs System Composition (Wet)

				164 H_2O							328 H_2O						
D−H[a]	species	A[b]	species	1:0:0	8:1:1	3:1:1	2:1:1	1:1:1	1:2:2	0:1:1	1:0:0	8:1:1	3:1:1	2:1:1	1:1:1	1:2:2	0:1:1
$-NH_2$	**A**	−O	**C**	−	19.3	17.2	14.6 7.	6.5	9.9	−	−	6.7	6.5	4.4	3.6	6.3	−
>CH	**A**	−O	**C**	−	12.0	5.0	2.2	5.4	4.3	−	−	4.1	2.9	3.4	2.9	3.7	−
$-NH_2$	**A**	−O	Tf_2N^-	23.0	21.6	20.2	19.3	20.1	19.3	−	21.4	19.8	20.6	21.3	19.6	19.7	−
>CH	**A**	−O	Tf_2N^-	11.0	10.7	10.1	11.2	8.2	9.4	−	10.5	9.3	9.8	7.9	8.8	7.2	−
$-NH_2$	**A**	>O	H_2O	15.3	12.5	8.8	9.8	6.5	7.4	−	10.8	9.8	9.3	8.3	10.0	8.5	−
$-NH_3$	**B**	−O	**C**	−	6.4	22.3	20.1	25.8	25.8	32.3	−	4.7	17.4	16.0	21.9	21.5	25.4
>CH	**B**	−O	**C**	−	5.1	1.0	5.9	4.0	9.1	7.2	−	1.8	2.9	4.1	2.6	8.2	6.5
$-NH_3$	**B**	−O	Tf_2N^-	−	20.6	18.8	17.2	17.9	19.7	18.0	−	18.4	12.1	14.8	13.9	16.1	14.6
>CH	**B**	−O	Tf_2N^-	−	7.8	9.0	9.5	6.5	7.0	8.3	−	8.9	8.0	8.4	7.6	7.1	6.0
$-NH_3$	**B**	>O	H_2O	−	12.9	11.7	11.9	9.8	11.0	11.5	−	18.9	19.5	16.2	14.4	13.0	15.0
>NH	**C**	−O	**C**	−	0.0	1.2	3.9	6.5	11.2	6.9	−	0.0	0.0	0.0	1.1	3.6	4.6
>CH	**C**	−O	**C**	−	11.2	6.1	10.5	12.7	21.4	19.4	−	5.8	7.1	5.3	13.3	14.0	13.5
>NH	**C**	−O	Tf_2N^-	−	15.2	9.4	15.4	15.3	14.4	17.3	−	12.9	8.2	14.3	17.7	15.8	17.2
>CH	**C**	−O	Tf_2N^-	−	10.7	10.0	11.2	8.3	8.5	9.5	−	7.0 .	9.6	10.7	7.7	6.4	9.6
>NH	**C**	>O	H_2O	−	0.8	5.0	2.5	3.1	3.3 3	3.6	−	6.3	10.8	5.7	2.9	8.5	4.0
OH_2	H_2O	$-NH_2$	**A**	25.6	26.3	20.4	12.7	9.7	12.3	−	37.6	35.9	32.3	27.7	27.3	22.9	−
OH_2	H_2O	−O	**C**	−	83.7	92.7	88.0	79.6	66.9	59.1	−	132	137	123	111	115	97
OH_2	H_2O	−O	Tf_2N^-	29.9	26.3	23.7	23.1	22.6	20.2	16.8	24.6	23.1	20.4	22.6	19.8	19.4	19.0

[a] Donor site (with D = N or C). $-NH_2$, $-NH_3$, and >NH are amine donor sites of **A**, **B**, and **C** respectively. >CH is donor site at the C2 position of the imidazolium ring. [b] Acceptor site. −O is acceptor site of **C** or Tf_2N^-. **Note**: >CH (D−H) interaction with H_2O (A) not significant for species **A**, **B**, and **C** (<5%) and are not included.

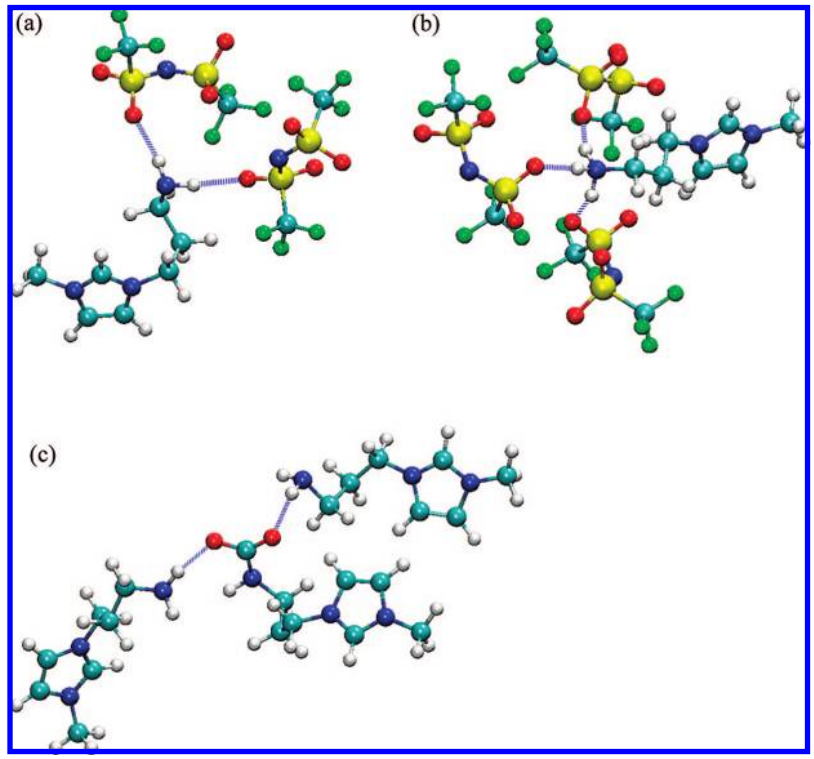

Figure 6. Amine ($-NH_2$) and ammonium ($-NH_3$) donor interactions with −O acceptor sites of Tf_2N^- (a,b) and **C** (c) in the 3:1:1 system.

hydrogen bonds, when viewed over the course of a typical simulation (several nanoseconds), remain locked in place and persist for very long periods of time. Thus, the **B** and **C** species cease to behave as discrete units but act rather as larger polymers or clusters. These **B** and **C** interactions are entirely consistent with the "salt-bridges" and polymeric structures described by Rudkevich and co-workers[24] and may therefore be classified as a manifestation of the same phenomenon. The translational and rotational motion of these larger units and their interactions with neighboring molecules explains the high experimental viscosities.[22,38] Figure 9c highlights the ammonium−carbamate tail interactions in the liquid as isolated green and red moieties (backbone atoms hidden) that form extended chains and clusters interspersed throughout the bulk. These structures are reminiscent of the nanoscale ordering observed in conventional ILs that is driven by hydrophobic/hydrophilic interactions. The difference is that the interactions in the TSIL system are stronger, more directional, and longer lived due to hydrogen-bonding.[50,51]

Table 6 shows the effect of water molecules on the hydrogen-bonding between the major **A**, **B**, **C**, and Tf_2N^- species. Interestingly, donor interactions (both nitrogen and carbon) from

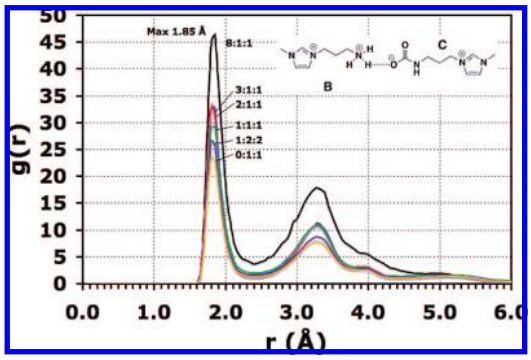

Figure 7. Site−site radial pair distribution function for **B**···**C** hydrogen-bonding interaction at different system compositions.

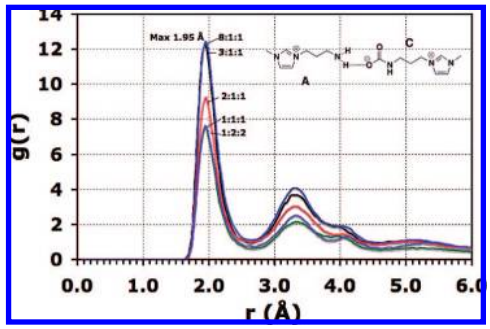

Figure 8. Site−site radial pair distribution function for **A**···**C** hydrogen-bonding interaction at different system compositions.

A, **B**, and **C** with the Tf_2N^- acceptor sites are minimally affected by the presence of water at both water contents. This indicates that the competitive effect between H_2O and the anion is small. Water hydrogens form a significant number of hydrogen bonds with the oxygen sites of the Tf_2N^- anion, as shown by the last entry in Table 6, on the order of 15−30% occupancy of available sites. However, there are a large number of oxygen donor sites (four) on each anion. As a result, competition for sites does not affect the **A**, **B**, and **C** interactions to a large extent.

Due to the large number of H_2O molecules relative to the number of **C** species, particularly in the 328 H_2O molecule systems, H_2O acts as a competitive donor for −O termini in the **C** species, and this is readily observable from the reduced occupancy percentages. The interactions of the >CH donor sites with −O from **C** fall off tremendously from competition, likely due to this being the weakest of the interactions. Likewise, the **A**···**C** interactions ($-NH_2$ with −O) are considerably lower in the 8:1:1 wet system versus the dry system at both water contents. In the 3.4 wt % system, there is a sharp tail-off to about 10% occupancy, while in the 6.5 wt % system, it remains constant at about 6%. Water donor interactions with the amine acceptor of **A** tail off from 25−35% at low CO_2 loading and fall off as **A** disappears.

The **B**···**C** interactions ($-NH_3$ with −O), which had an extremely high percentage occupancy of 51.7% in the dry 0:1:1 system, now attain a maximum of only about 25−30% occupancy at both water concentrations in the fully reacted system. Although this occupancy still very high, there is obvious competition with H_2O molecules for the very nucleophilic −O

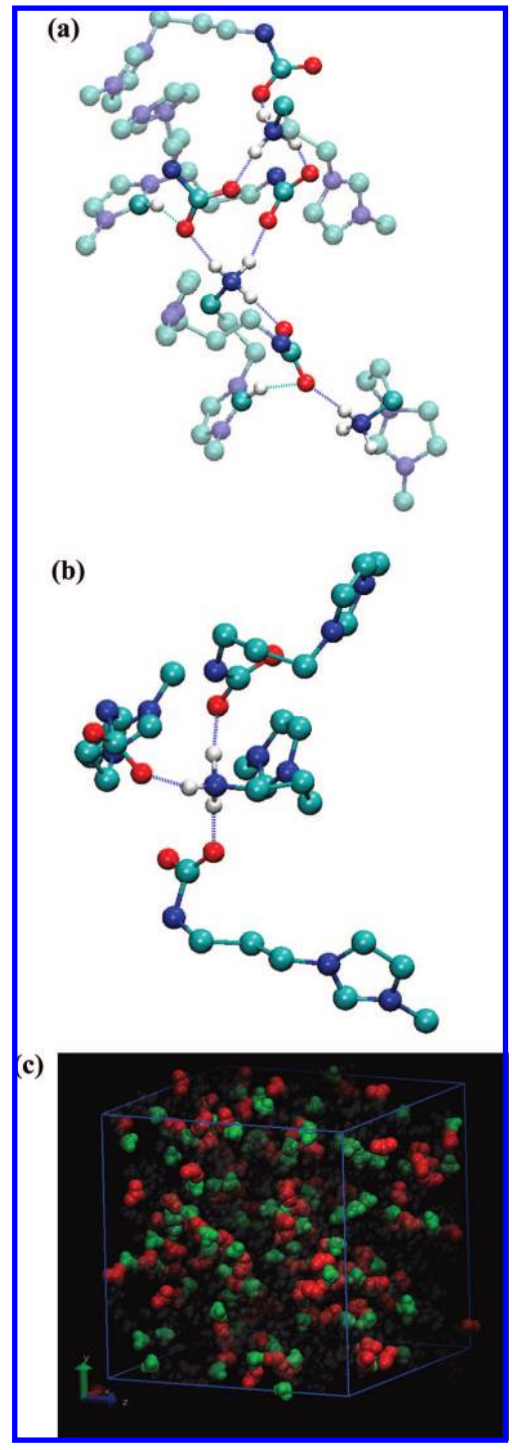

Figure 9. Examples of **B**···**C** hydrogen-bonding interactions in the 0:1:1 system (a) and the 1:2:2 system (b), including a simulation box perspective of these interactions in the 0:1:1 system (c), with **B** tails labeled green and **C** tails labeled red.

sites of **C**. The degree to which H_2O competes is evident from the OH_2 donor interactions with the −O acceptor site of **C**. At 3.4 wt % water, a tremendous number of these sites are occupied, ranging from 92.7% down to 59.1% of total possible sites. As discussed previously, many of these may be bifurcated. Astonishingly, at 6.5 wt % water, the occupancy percentages fall in the range of 137% down to 97%. Overwhelming numbers of H_2O relative to **C** species are responsible at low CO_2 loading, while there is more competition at higher CO_2 loading due to

(50) Jiang, W.; Wang, Y.; Voth, G. A. *J. Phys. Chem. B* **2007**, *111*, 4812–4818.
(51) Canongia Lopes, J. N. A.; Padua, A. A. H. *J. Phys. Chem. B* **2006**, *110*, 3330–3335.

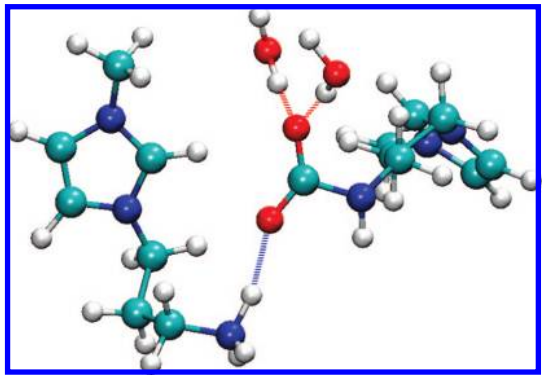

Figure 10. Bifurcated hydrogen-bonding of H_2O molecules with **C** in the 1:2:2 system, including a **B**···**C** hydrogen-bonding interaction.

larger number of **C**, hence the lower occupancy of 97%. These occupancy percentages fall above the 100% threshold assumed by a 1:1 saturation value due to a large number of bifurcated sites. This is clearly evident in Figure 10, showing how **C** can share its −O termini with **B** and two bifurcated water molecules. These results are entirely consistent with the MSD vs time, D_s, and τ calculations previously discussed. The lower fraction of **B**···**C** occupancies coincides with the enhanced dynamics due to the presence of water in the reacted systems. In addition, the decrease in the dynamics of the pure TSIL (1:0:0) upon addition of H_2O (an unexpected result) can be attributed to the large number of hydrogen-bonding interactions between the $-NH_2$ terminus and water molecules. It should be noted that the strength of the hydrogen-bonding interactions between H_2O and **A**, **B**, **C**, or Tf_2N^- is likely too high due to the nature of SPC water model, which was parametrized from bulk water.[45] The less polar ionic liquid environment[52] would likely require dampened charges or a polarizable model to obtain greater accuracy. Nevertheless, it is clear that the hydrogen-bonding network observed in the simulations is very likely the cause of the observed increase in viscosity with the addition of CO_2.

Conclusions

Molecular dynamics simulations were performed to study the static and dynamic properties of an imidazolium-based amine-tethered task specific ionic liquid (TSIL) that is being investigated for CO_2 gas capture. Classical force fields were developed to describe the pure TSIL as well as the species formed upon reaction with CO_2, including quaternary ammonium and carbamate species. Several reaction mixture compositions, both dry and with water present, were studied that represent varying amounts of reacted CO_2. The ability of the force field to predict the densities of the reaction mixtures is unknown due to the difficulty in performing the experimental measurements, but the pure TSIL density was determined accurately. The reliable quantitative calculation of the self-diffusion coefficients and rotational time constants for all of the species in the various mixture compositions proved to be intractable due to the extremely slow dynamics of the system. The addition of water molecules to the simulations increased the dynamics in nearly all cases, but they still remained sluggish. Qualitatively, the results predict that the reaction of CO_2 with the TSIL results in the formation of gel-like or glassy materials, even at very low CO_2 mole fractions. This finding is consistent with experimental observations.[22] Detailed hydrogen bond analysis showed a direct correlation between the slow system dynamics and the formation of strong, dense hydrogen-bonded networks, primarily between the zwitterion (**C**) and dication (**B**) species formed upon reaction of CO_2 with the TSIL cation. This phenomenon is consistent with the formation of salt bridges observed following the reaction of CO_2 with amine-tethered supramolecular architectures.[24]

The nature of the TSIL system upon its reaction with CO_2 has significant implications for the design and implementation of CO_2 capture processes. The slow dynamics observed during the simulation are consistent with experimental observations of gel-like materials and measurements of extremely high viscosities upon CO_2 complexation.[22,38] Such viscous, gel-like materials pose an engineering challenge for processes based on continuous-flow systems. However, due to the high degree of tunability and the large number of potential ILs,[53] ample opportunity exists to overcome these challenges and improve their properties. For example, introducing alternative reactive functionalities into the cation or altering the identity of the cation altogether (i.e., to pyridinium, ammonium, or phosphonium) will undoubtedly result in materials with entirely different physical properties. Likewise, introducing the CO_2-reactive moiety into the anion rather than the cation, such as in an amino acid-derived TSIL based on glycine, will enlarge the portfolio of IL candidates and potentially alter the reaction mechanism.

An alternative to chemical modification is the use of mixtures of ionic liquids. Binary mixtures of reactive TSILs with nonreactive ILs, such as 1-butyl-3-methylimidazolium bis(trifluoromethanesulfonyl)imide, offer not only the promise of lower viscosities but also lower costs associated with the conservation of expensive, specialized TSIL materials. Likewise, binary or ternary mixtures that involve TSILs combined with organic diluents, such as in IL−liquid clathrate systems,[54] offer a plethora of alternatives and potential solutions. In the case of organic diluents, careful control of solvent polarity can be a powerful tool in moderating the strength of the salt-bridge interaction, and hence controlling the viscosity of the CO_2-reacted system.

The high viscosity of amine-tethered TSILs before and after complexation with CO_2 is not entirely a hindrance. TSILs that have been deposited or supported on a porous matrix within a membrane, also known as supported ionic liquid membranes (SILMs), have been shown to exhibit high permeability and selectivity for CO_2.[55] High viscosity in this instance is desirable, and selectivity has been shown to increase with increasing temperature over a particular range. Significant opportunities exist to fine-tune membrane performance by altering the strength of the CO_2 complex.

In addition to direct applications to CO_2 capture and sequestration, the dynamic changes in the liquid structure of the TSIL as the fraction of complexed CO_2 increases offer a particularly unique opportunity to probe solvation dynamics of small molecules in a heterogeneous environment. Maroncelli and co-workers demonstrated that distinct structural heterogeneities exist in traditional ionic liquids, presumably due to their inherent conformational flexibility, that, when combined with their slow relaxation compared to many other solvents, can

(52) Daguenet, C.; Dyson, P. J.; Krossing, I.; Oleinikova, A.; Slattery, J.; Wakai, C.; Weingartner, H. *J. Phys. Chem. B* **2006**, *110*, 12682–12688.
(53) Rogers, R. D.; Seddon, K. R. *Science* **2003**, *302*, 792–793.
(54) Holbrey, J. D.; Reichert, W. M.; Nieuwenhuyzen, M.; Sheppard, O.; Hardacre, C.; Rogers, R. D. *Chem. Commun.* **2003**, 476–477.
(55) Myers, C.; Pennline, H.; Luebke, D; Ilconich, J.; Dixon, J. K; Maginn, E. J.; Brennecke, J. F *J. Membr. Sci.* **2008**, *322*, 28–31.

provide a medium in which to probe or control chemical processes at the molecular level.[56] The enhanced degree of solvent tunablility via CO_2 complexation with the TSIL offers a unique opportunity to control the heterogeneity of ionic liquids even further.

It is hoped that these calculations, which provide a mechanistic explanation for the empirical observations that CO_2 complexation causes a dramatic increase in amine-functionalized ionic liquid viscosity, will stimulate future computational and experimental studies on these systems.

Acknowledgment. This material is based upon work supported by the U.S. Department of Energy under Award No. DE-FC26-07NT43091.

Supporting Information Available: Complete ref 27; atom types and force field parameters for species **A**, **B**, and **C**; and initial configuration dependence results. This material is available free of charge via the Internet at http://pubs.acs.org.

JA804654B

(56) Jin, H.; Li, X.; Maroncelli, M. *J. Phys. Chem. B* **2007**, *111*, 13473–13478.